Propagation Characteristics in Indoor Scenario with Different Transmitter Locations at 3.5 and 6 GHz

Xinzhuang Zhang[1(✉)], Yawei Yu[1], Lei Tian[1], Yu Han[1], Yu Zhang[3], and Jianhua Zhang[1,2]

[1] Key Lab of Universal Wireless Communications, Ministry of Education, Beijing University of Posts and Telecommunications, Mailbox NO. 92, Beijing 100876, China
{zxzhuang,tianlbupt,jhzhang}@bupt.edu.cn

[2] State Key Laboratory of Networking and Switching Technology, Beijing University of Posts and Telecommunications, Mailbox NO. 92, Beijing 100876, China

[3] Qualcomm Inc., 6/F, Tower C, Beijing Global Trade Center, 36 North 3rd Ring East Road, Beijing 100013, China
zhangyu@qti.qualcomm.com

Abstract. This paper presents results from the measurement in indoor conference scenario at 3.5 GHz and 6 GHz. The measurement was performed by using multiple-input multiple-output (MIMO) antennas including uniform planar array (UPA) at transmitter end (Tx) and omni-directional array (ODA) at receiver end (Rx). Two cases including UPA on the wall and the ceiling, have been measured and comprehensive propagation characteristics have been investigated in detail. Based on the measurement, delay and spatial parameters are analyzed and then compared with the standard model. The delay spread measured shows smaller value than standard model due to the small size of the scenario and the elevation angle spread is presented for establishing three-dimensional (3D) channel model. Further, the capacity performances of the channel in different cases are evaluated, and the results indicate that the system with transmitter antenna mounted on the wall performs better.

Keywords: MIMO channel · Elevation angle spread
Channel capacity

1 Introduction

With the continuous development of mobile internet, as well as the emergence of new technology such as Virtual Reality (VR) and Augmented Reality (AR), the demand for data rate has increased greatly. The fifth generation (5G) communication has been widely researched to provide higher data rate and frequency efficiency to satisfy this requirement in the near future. MIMO technology has

K. Long et al. (Eds.): 5GWN 2017, LNICST 211, pp. 640–649, 2018.
https://doi.org/10.1007/978-3-319-72823-0_59

been verified as a key technology for 5G system. In order to achieve better performance of the technology, understanding the MIMO channel characteristics deeply is necessary. The field measurement is an essential way to obtain the channel properties. Meanwhile it can also provide guideline for system designing and network planning.

As an important deployment scenario for 5G, indoor scenario has been depicted in 3GPP TR 36.900 [1]. So the study of channel characteristics and modeling in indoor scenarios arises researchers' great interests. There are plenty of measurements conducted by different researchers for various channel environments. In [2], the comparison of channel parameters at 3.5 GHz in room-room, room-corridor and corridor-corridor cases was made, the result indicates that the root mean square delay spread (rms DS) in corridor-corridor case has the maximum value for existing obvious reflection paths. And in [3], Central Hall as indoor scenario was measured at three frequency band including 2 GHz, 4 GHz and 6 GHz, and the analysis results demonstrate that the delay spread has no clear dependency on carrier frequency.

In [1], indoor scenarios include office environments and shopping malls, with transmitter antennas mounted on the ceilings or walls. However, there is little literature on investigating the channel characteristics difference between dissimilar Tx location in indoor environment. The attention should be paid more on that.

In this paper, propagation characteristics in indoor conference scenario at 3.5 GHz and 6 GHz were investigated. Two cases including Tx antenna array on the wall and on the ceiling have been measured in detail. We present and compare the key channel parameters such as delay spread and angle spread in two cases. Further, the performances of antenna system in two cases are discussed. The results can provide guideline for 5G communication system design, especially for small cell system.

The rest of this paper is organized as follows. Section 2 gives a detailed description of the measurement campaign. Data post process methods are introduced in Sect. 3. Then analysis results follow in Sect. 4 and Sect. 5 draws the conclusions.

2 Measurement Description

2.1 Measurement System

In field measurement, the channel sounder described in [4] was utilized to conduct the measurement campaign. It consists of three units: transmitter sounder, receiver sounder, and receiver baseband processing unit (RBPU). The RBPU is used to store the raw data received by the receiver sounder. With different radio frequency converter placed in the sounders, measurement at different frequency band such as 3.5 GHz and 6 GHz can be achieved. To capture propagation rays in 3D environment efficiently, full dimensional arrays are equipped at both sides of a measurement link. During our field measurements, dual-polarized ($\pm 45°$) ODA consisting of 56 antenna elements is used at the Rx, while UPA with 32 antenna

elements at the Tx, as described in Fig. 1. The array elements are microstrip patches and their 6 dB beamwidths are approximately 110° in both vertical and horizontal planes. The gain of each antenna element is 6 dBi, and angle resolution is 2°. In Table 1, measurement parameters including antenna height are listed.

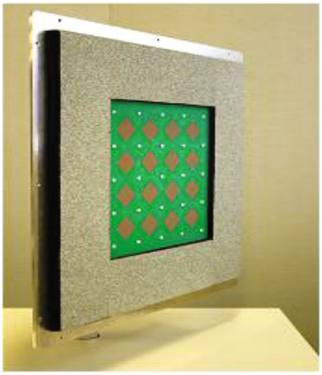

(a) UPA (Tx)

(b) ODA (Rx)

Fig. 1. Layout of antenna arrays

Table 1. The specifications of measurement

Items	Tx-W	Tx-C
CF (GHz)	3.5/6	3.5/6
Bandwidth (MHz)	100	100
Length of PN code (Chips)	127	127
Transmitter antenna/Number	UPA/32	UPA/32
Receiver antenna/Number	ODA/56	ODA/56
Polarized	±45°	±45°
Height of Tx antenna (m)	1.8	2.4
Height of Rx antenna (m)	1.2	1.2

2.2 Measurement Scenario

We carried out the field measurement for 3D channel impulse response (CIR) in a conference room for indoor scenarios. The room is 5.85 m long, 5.10 m wide and 2.40 m high with gypsum ceiling and concrete block wall. And there are no windows in the room. In the middle, there is a long wooden table. The UPA is fixed on different locations-the wall and the ceiling, namely Tx-W and Tx-C case, respectively. The UPA location for Tx-C case is showed in Fig. 2(a).

And the ODA is positioned at the marked spots from number 1 to 20 for static measurement in each case, as depicted in Fig. 2(b). There is no obstruction between transmitter and receiver, so all the measurements are line of sight (LoS) condition. For each case and each central frequency, approximately 20 different spots are measured with 500 snapshots collected for each spot.

(a) The Propagation Environment in Tx-C case for UPA

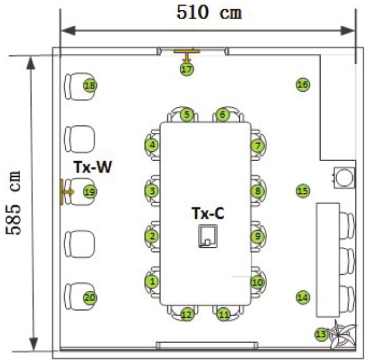

(b) The location of the measured spots for two cases

Fig. 2. The overview of the measurement scenario

3 Data Post-processing

After measurement, post processing is implemented with two steps: firstly, obtaining CIR from the measured raw data; then extracting channel parameters such as delay, power and angle from CIR. The CIR is converted from the raw data through eliminating the system impulse response by correlating the received signals with calibration signal. When extracting channel parameters, channel model needs to be introduced. The 3D channel model for LTE has been introduced in 3GPP TR 36.873 [5] and for any given delay τ, it is given by

$$h_{u,s}(\tau_l;t) = \sum_{l=1}^{L} \begin{bmatrix} F_{rx,u,\theta}(\mathbf{\Omega}_l) \\ F_{rx,u,\phi}(\mathbf{\Omega}_l) \end{bmatrix}^T \begin{bmatrix} \alpha_{l,\theta,\theta} & \alpha_{l,\theta,\phi} \\ \alpha_{l,\phi,\theta} & \alpha_{l,\phi,\phi} \end{bmatrix} \begin{bmatrix} F_{tx,s,\theta}(\mathbf{\Phi}_l) \\ F_{tx,s,\phi}(\mathbf{\Phi}_l) \end{bmatrix} \times \exp(j2\pi\lambda_0^{-1}(\mathbf{\Omega}_l \cdot \bar{r}_{rx,u})) \exp(j2\pi\lambda_0^{-1}(\mathbf{\Phi}_l \cdot \bar{r}_{tx,s})) \times \exp(j2\pi f_{d,l}t) \quad (1)$$

Where, L is the total number of multiple components (MPC), λ is the wavelength of the carrier frequency. The SAGE algorithm [6] is applied in order to estimate channel parameters from CIRs. As an extension of the maximal likelihood estimation (MLE) algorithm, taking the antenna pattern into account, the SAGE algorithm provides a joint estimation of the parameter set, $\theta_l = \{\tau_l, \mathbf{\Phi}_l, \mathbf{\Omega}_l, f_{d,l}, \mathbf{A}_l\}, l = 1, 2, ..., L$, where τ_l, $f_{d,l}$, $\mathbf{\Phi}_l$, $\mathbf{\Omega}_l$ and $\boldsymbol{A}_l$ denote the propagation delay, the Doppler shift, the direction of departure, the direction

of arrival, and the complex polarization matrix of the lth path, respectively. Specially, $\mathbf{\Phi}_l = (\theta_{T,l}, \phi_{T,l})$, $\mathbf{\Omega}_l = (\theta_{R,l}, \phi_{R,l})$, where $\theta_{T,l}$, $\phi_{T,l}$, $\theta_{R,l}$ and $\phi_{R,l}$ denote the elevation of departure (EoD), azimuth of departure (AoD), elevation of arrival (EoA), and azimuth of departure (AoA) of the lth path, respectively. For each measurement snapshot, $L = 200$ paths are estimated by the SAGE algorithm.

3.1 Delay Parameters

The main parameters of time domain dispersion include mean excess delay τ_{mean} and rms DS τ_{rms}. They can be determined from a power delay profile (PDP). The rms DS is defined as the root mean square of second central moment of the power delay profile. So rms DS can be calculated as below [7]

$$\tau_{rms} = \sqrt{\frac{\sum_l (\tau_l - \tau_{mean})^2 P_l}{\sum_l P_l}} \tag{2}$$

where

$$\tau_{mean} = \frac{\sum_l \tau_l P_l}{\sum_l P_l} \tag{3}$$

These delays τ_l are measured relative to the first detective arriving path at the receiver.

3.2 Spatial Parameters

Root mean square angle spread σ_{AS} is a key factor to characterize the dispersion in spatial domain. As mentioned in the former part of Sect. 3, the azimuth and elevation angles of the MPC can be extracted from CIRs. The mean angle spread $\mu(\Delta)$ and the circular angle spread (CAS) [8] σ_{AS} can be calculated by [7]

$$\sigma_{AS} = \min_{\Delta} \sigma_{AS}(\Delta) = \sqrt{\frac{\sum_{l=1}^{L} (\phi_l(\Delta) - \mu(\Delta))^2 P_l}{\sum_{l=1}^{L} P_l}} \tag{4}$$

$$\mu(\Delta) = \frac{\sum_{l=1}^{L} \phi_l(\Delta) P_l}{\sum_{l=1}^{L} P_l} \tag{5}$$

$$\phi_l(\Delta) = \phi_l + \Delta \tag{6}$$

$$\phi_l = \begin{cases} 2\pi + \phi_l & \phi < -\pi \\ \phi_l & |\phi| \le \pi \\ 2\pi - \phi_l & \phi > \pi \end{cases} \tag{7}$$

where L, P_l, and $\phi_l(\Delta)$ denote the number of paths, the power of the lth path and the angle of the lth path adding a shifted angle which denotes a certain angular shift.

3.3 Channel Capacity

The channel capacity is an important metric of the MIMO channel. For the CIR of each measurement location, the Discrete Fourier Transform is applied to obtain the channel response matrix $\boldsymbol{H}_{U,S}(f;t)$, where f denotes the subcarrier indice. The mean capacity of frequency selective fading channel over all subcarriers at all fixed spots of different ones is given [9] by

$$C = \frac{1}{Q}\sum_{q=1}^{Q} \log_2 \det(I_N + \frac{\rho}{\beta M} H_{u,s,q} H_{u,s,q}^H) \tag{8}$$

Where Q is the number of channel realizations, ρ is the signal to noise ratio (SNR) and β is a common normalization factor for all channel realizations within one snapshot which satisfies

$$E[\frac{1}{\beta}\|H_{u,s,q}\|_F^2] = US \tag{9}$$

where $\|\bullet\|_F^2$ denotes the Frobenius norm.

4 Results of Measurements

4.1 Delay Characteristics

Delay spread expresses the delay dispersion of the channel and is probably the most important metric describing a radio channel characteristics. When considering delay spread from PDP, the noise cut threshold has to be mentioned. A 20 dB noise threshold criterion [10] has been utilized meaning that incoming paths with higher than 20 dB power difference compared to the most powerful path have been removed. According to the former part, the rms DS is obtained for two cases, and then summarized in Table 2. CF denotes central frequency. The mean excess delay and rms DS obey the lognormal distribution. For example, the fitted cumulative probability density curve of the rms DS obtained in Tx-C case at 6 GHz is depicted in Fig. 3.

From the Table 2, we can observe that the mean excess delay's variation range is from 20 ns to 28 ns in all cases. And in Tx-C case at 3.5 GHz it is smaller than that in Tx-W case, while at 6 GHz, it shows opposite tendency in

Tx-W case. So there is no obvious changing rules for excess delay when Tx location vares. In terms of rms DS, the values in two cases are almost the same, for the tiny difference in a few nanoseconds can be ignored. So there are no obvious dependency between rms DS and frequency. Compared to the InH scenario in [10], the value is smaller as a result of the small size of the room.

Table 2. Delay parameters for two cases

CF (GHz)	3.5		6		3.4
Case	Tx-C	Tx-W	Tx-C	Tx-W	InH
τ_{mean} (ns)	20.08	24.00	28.37	22.68	N/A
τ_{rms} (ns)	10.41	13.38	14.23	13.50	19.95

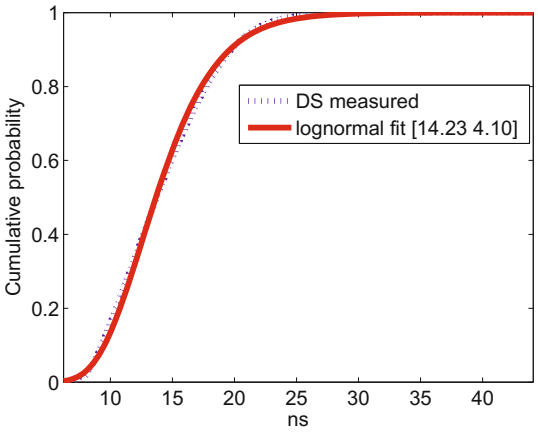

Fig. 3. Fitting results of DS in Tx-C case at 6 GHz

4.2 Spacial Characteristics

The rms AS including EoD, EoA, AoD and AoA can be calculated according to Eqs. 4, 5, 6 and 7 in Sect. 3.2 and the mean values of rms angle spread for Tx-C and Tx-W cases are listed in Table 3.

It is easily observed that arrival angle spread is larger than departure angle. For example, ASA is greater than ASD in Tx-C case as well as Tx-W case. This is due to that Tx antenna is mounted at one place while Rx antenna is set along the measured route so receiver enjoys more scatters than transmitter. As we predict, AS decreases when the frequency increases in a given case, for arrival azimuth angle spread shows greater value at 3.5 GHz than that at 6 GHz in identical case. It is due to the fact that the smaller the wavelength of carrier is, the less scattering paths arrive at the receiver. It is worth noting that ESA

Table 3. The statistical spatial parameters in two cases

CF (GHz)	3.5		6		3.4
Case	Tx-C	Tx-W	Tx-C	Tx-W	InH
ASD (°)	30.2	33.8	28.8	25.7	39.8
ESD (°)	24.0	30.2	26.9	26.9	N/A
ASA (°)	53.7	58.8	50.1	51.3	41.7
ESA (°)	27.5	42.6	26.9	38.9	N/A

in Tx-C case is much smaller than that in Tx-W case at 3.5 GHz and 6 GHz. It is resulted from the fact that there are more reflection and scattering paths from the walls and table arriving receiver when the UPA is equipped on the wall. As for ASA, the variation is not obvious. Above all, in conference room, the Tx antenna location has an obvious influence on angle spread, especially for elevation angle. The deep understanding of spacial parameter can be utilized for beamforming.

4.3 Capacity Analysis

Using the channel matrix H from the CIR, channel capacity can be obtained by Eq. 8. The capacities were calculated in two cases to predict the capacity in conference scenario. For the inter element spacing impacts the capacity, here half wavelength spacing is adopted for 3.5 GHz and 6 GHz, respectively.

From Fig. 4, the antenna-on-wall system performs better compared to the antenna-on-ceiling system no matter at 3.5 GHz or 6 GHz. At an SNR of 30 dB, the antenna-on-wall system at 3.5 GHz provides an ergodic capacity of

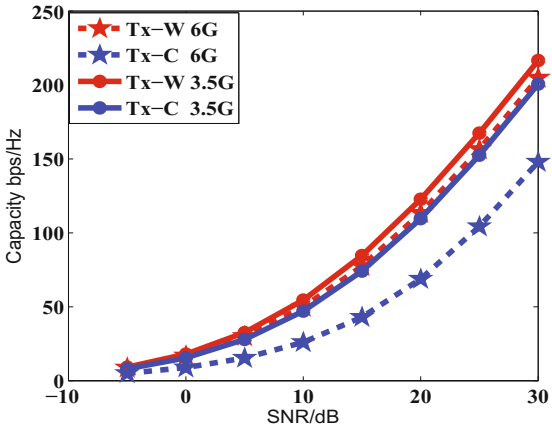

Fig. 4. The capacity of 56 receiving antenna and 32 transmitting antenna

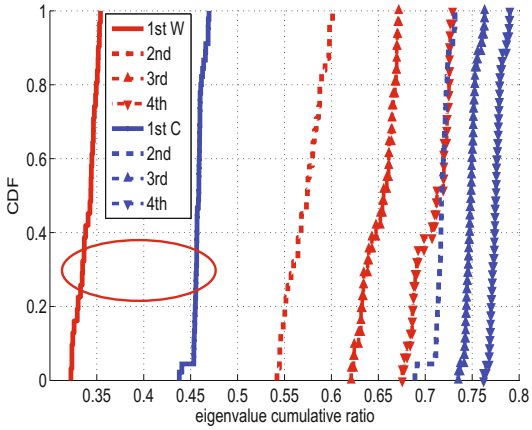

Fig. 5. The cumulative ratio of eigenvalues of channel for two cases at 3.5 GHz

216.5 bits/s/Hz. It is known that channel correlation between subchannels impacts the channel capacity. So the eigenvalues of the MIMO channel were analyzed to find the reason. We chose spot 7 described in Fig. 2(b) for example. The CDF curves for cumulative ratio of the first four eigenvalues in Tx-C case and Tx-W case are depicted in Fig. 5. As emphasized by the rad ellipse, We can find that the main eigenvalue in Tx-C case is larger than that in Tx-W case, indicating antenna system in Tx-W case has lower correlation between subchannels, so it obtains better capacity performance.

5 Conclusion

In this paper, we have reported the results from the measurement in indoor conference scenario. The 3.5 GHz and 6 GHz frequency bands are candidate bands for 5G system, and the measurement scenario is of importance to indoor scenarios.

In LoS condition, two cases including Tx antenna array on the wall and the ceiling at 3.5 GHz and 6 GHz have been measured with UPA and ODA to obtain delay and spacial domain parameters, as well as capacity performance. We compared channel characteristics in two cases in detail. For delay domain dispersion parameters, rms DS has no clear dependency on frequency, and the values are around 14 ns in two cases. For spacial domain parameters, elevation arrival angle spread shows a large difference between Tx-W and Tx-C case, and in Tx-C case it is about ten degrees larger than that in Tx-W case. And the MIMO system with transmitter antenna on the wall has a better performance at 3.5 GHz, obtaining up to 216.5 bits/s/Hz. So transmitter antenna mounted on the wall may be a good choice for indoor small cell system deployment.

Acknowledgments. This research is supported in part by National Science and Technology Major Project of the Ministry of Science and Technology (2015ZX03002008), and by National Natural Science Foundation of China (61322110, 6141101115), and by Doctoral Fund of Ministry of Education (20130005110001), and by Qualcomm Incorporated.

References

1. 3GPP TR 36.900: Study on Channel Model for Frequency Spectrum above 6 GHz (Release 14) (2016)
2. Zeng, J., Zhang, J.: Propagation characteristics in indoor office scenario at 3.5 GHz. In: 8th International ICST Conference on Communications and Networking in China (CHINACOM), Guilin, pp. 332–336. IEEE Press (2013)
3. Li, J., et al.: Measurement-based characterizations of indoor massive MIMO channels at 2 GHz, 4 GHz, and 6 GHz frequency bands. In: 83rd Vehicular Technology Conference (VTC Spring), Nanjing, pp. 1–5. IEEE Press (2016)
4. Zhang, J.: Review of wideband MIMO channel measurement and modeling for IMT-advanced systems. Chin. Sci. Bull. **57**(19), 2387–2400 (2012)
5. 3GPP TR 36.873: Study on 3D Channel Model for LTE (Release 12) (2014)
6. Fleury, B.H., Jourdan, P., Stucki, A.: High-resolution channel parameter estimation for MIMO applications using the SAGE algorithm. In: International Zurich Seminar on Broadband Communications Access - Transmission - Networking, Zurich, p. 30-1 (2002)
7. Rappaport, T.S.: Wireless Communications: Principles and Practice. Prentice Hall, New Jersey (2001)
8. 3GPP TR 25.966: Spatial Channel Model for Multiple Input Multiple Output (MIMO) Simulations (2003)
9. Yu, K., Bengtsson, M., Ottersten, M., McNamara, D., Karlsson, P., Beach, M.: Modeling of wide-band MIMO radio channels based on NLoS indoor measurements. IEEE Trans. Veh. Technol. **53**(3), 655–665 (2004)
10. ITU-R M.2135: Guidelines for Evaluation of Radio Interface Technologies for IMT-Advanced (2009)